Limnol. Oceanogr., 43(1), 1998, 34–43

Theory and measurements of the complete beam spread function of sea ice

Robert A. Maffione[1]
Hydro-Optics, Biology, and Instrumentation Laboratories, Moss Landing, California 95039-0859

Jeff M. Voss
SRI International, Menlo Park, California 94025

Curtis D. Mobley
Sequoia Scientific, Mercer Island, Washington 98040

Abstract

The beam spread function (BSF) of sea ice is of interest for several reasons. The BSF characterizes beam propagation through sea ice. Its equivalent, the point spread function, is essentially the optical impulse response of the medium, which has many useful connections to radiative transfer theory. In-ice measurements of the BSF over the full angular range 0–180°, using a novel method, were made of first- and multiyear ice off the shore of Barrow, Alaska. All of the measured sea ice BSFs were drastically different than the BSF of ocean water, and they strongly indicated that sea ice is a highly scattering medium, with a single scattering albedo generally >0.97 over the visible spectrum. At pathlengths >30 cm, the BSF was found to be nearly identical to the computed asymptotic radiance distribution. The rapid approach to the asymptotic state and the high single scattering albedo of sea ice suggest that photon diffusion theory should accurately describe radiative transfer in sea ice away from boundaries. Equating the results of diffusion theory with asymptotic radiative transfer theory yields a simple expression that relates the asymptotic attenuation coefficient K_∞ to the inherent optical property coefficients and the asymmetry parameter g of the scattering phase function. It is shown that the necessary optical parameters for computing g can be obtained from the measured BSF. Thus, all the information necessary for modeling optical propagation in sea ice can be obtained from the BSF measurements using the method described here.

Sea ice is generally a highly scattering optical medium. Its physical structure is highly complex as well, consisting of a usually unknown distribution of air bubbles, irregularly shaped brine pockets, fractures, and embedded particles, which all strongly scatter light (Perovich and Gow 1991). Measuring the optical properties of sea ice is equally challenging owing to its solid nature and the usually harsh working conditions. Thus, sea ice remains one of the least understood natural optical media.

To characterize the optical properties of sea ice, researchers usually have taken an approach similar to that employed for characterizing the optical properties of ocean water, but with greater limitations. For example, the spectral solar irradiance attenuation through sea ice has been measured and the results characterized by bulk irradiance attenuation coefficients for the entire slab of ice (Grenfell and Maykut 1977; Maykut and Grenfell 1975; Perovich et al. 1986). In fact, nearly all optical measurements of sea ice in the field have involved ambient light measurements, from which apparent optical properties (AOPs) of sea ice can be directly computed. These measurements and the resultant AOPs are useful for characterizing optical propagation through sea ice, but they suffer from the same difficulties of interpretation as do AOPs of ocean water.

Obtaining data on the inherent optical properties (IOPs) of sea ice is highly desirable because IOPs yield information about the fundamental optical nature of the medium. Moreover, IOPs are necessary input for radiative transfer models of light propagation in sea ice (Grenfell 1991; Perovich and Grenfell 1982). But sea ice IOPs are exceedingly difficult to measure, even in the laboratory (Light 1995; Perovich and Grenfell 1981). Nonetheless, a few researchers have made heroic attempts at measuring sea ice IOPs, including the absorption coefficient (Grenfell and Perovich 1981; Perovich and Govoni 1991; Roesler and Iturriaga 1994) and the scattering phase function (Grenfell and Hedrick 1983; Miller et al. 1994). Thus far, however, reported results remain preliminary, especially regarding the IOPs of natural sea ice.

The beam spread function (BSF) and its mathematical equivalent, the point spread function (PSF), are useful radiometric functions for characterizing an optical medium (Mertens and Replogle 1977). The BSF is defined as the irradiance distribution due to a collimated beam as a function of distance R and polar angle θ from the source, normalized by the source power, or radiant flux. The PSF is defined as the radiance distribution due to a plane Lambertian source, as a function of R and θ, normalized by the source power divided by π (i.e. the PSF is normalized by the maximum source intensity) (*see* Mertens and Replogle [1977] for a thorough description of these two functions). Although it was known for some time that the properly defined PSF and

[1] Part of this work was conducted while the author was a graduate student at Oregon State University.

Acknowledgments

Special thanks are given to Scott Pegau and Jessie Collins for their help in collecting the BSF data. This work was funded by the Environmental Optics Program at the Office of Naval Research and was part of ONR's departmental research initiative, Electromagnetic Properties of Sea Ice.

BSF are equal (Honey 1979), a rigorous proof was only recently given by Gordon (1994).

The PSF is fundamental to imaging (Wells 1969), and the BSF has direct applications to laser propagation and lidar (Honey 1979). Small-angle scattering theory relates the PSF to the volume scattering function (VSF) in the paraxial, or small-angle, approximation in a way that can be analytically inverted to obtain the VSF from the measured PSF (Wells 1969). Owing to the interest in underwater imaging and ocean lidar, considerable attention has been given to characterizing the PSF of ocean waters (Voss and Chapin 1990; Maffione et al. 1991), although there has been little progress at inverting the measured PSF to obtain the VSF using small-angle scattering theory (Voss 1991).

Because the PSF is essentially the radiance distribution due to a Lambertian source, it can be integrated to yield the scalar and planar irradiances. Maffione et al. (1993) have shown that the bulk absorption coefficient of the medium can be accurately determined from these two irradiance measurements as a function of distance from the source. No absolute calibration is needed, and furthermore the method is exact, so that its accuracy is unaffected by even a highly scattering medium. Thus, the method described below for measuring the complete BSF of sea ice, which is the equivalent PSF, can be integrated to yield both the scalar and net irradiances due to a Lambertian source. From these two irradiance quantities, the absorption coefficient, diffuse attenuation coefficient, and the average cosine of the light field can be determined.

The only reported attempt at measuring the PSF of sea ice was performed by Gilbert and Buntzen (1986) using a method developed by Honey (1979) and instrumentation developed by Moore (1985). Gilbert and Buntzen attempted to measure the bulk PSF of Arctic sea ice by lowering a Lambertian light source into the water below the ice and recording the radiance distribution emerging above the ice with a camera. Problems with their particular experimental method in the harsh arctic environment limited the usefulness of these measurements. Nonetheless, a subsequent analysis of the Gilbert and Buntzen data by Voss et al. (1992) showed that the PSF of sea ice is far broader than the PSF of ocean water, indicating a high degree of scattering by sea ice.

Measurements of the planar irradiance distribution due to a collimated source, which is a paraxial approximation to the BSF, were made of a slab of laboratory grown saline ice by Schoonmaker et al. (1989). Their results also showed that sea ice is a highly scattering medium. Schoonmaker et al. computed the BSF with forward and inverse Hankel transforms of their planar irradiance measurements. By using the same optical geometry as Schoonmaker et al., Longacre and Landry (1994) measured the planar irradiance distribution due to a beam propagating vertically through a bulk slab of Arctic sea ice. As in Schoonmaker et al.'s setup, Longacre and Landry's measurements were not strictly the BSF, but their results once again confirmed that sea ice is a highly scattering medium. Tanis (1994) also used a similar setup to make beam spreading measurements of sea ice samples taken from cores. Tanis's goal was to use his measurements in Wells's small-angle scattering inversion algorithm (Wells 1969) to obtain the small-angle VSF. However, recent investigations by Joelson (1996), using a Monte Carlo model, indicated that small-angle scattering theory breaks down for highly scattering media because these theories do not take into account the scattering of photons back into the forward light path. These theories take into account only multiple scattering that occurs within the paraxial angles (nominally $<10°$). It therefore does not appear that the small-angle VSF can be determined for sea ice with the Wells inversion algorithm due to the highly scattering nature of this medium.

A new method for measuring the BSF of sea ice is described. It is shown that this method allows the BSF to be measured over the full 180° range of polar angles in a manner that properly relates it to the strict definition of the BSF. This method is used to determine the BSF over horizontal paths of selected distances, as opposed to previous field techniques used for measuring an approximation of the BSF over vertical paths through the entire ice sheet. Moreover, the horizontal-path BSF can be measured as a function of depth within the ice. This method was tested near Barrow, Alaska, in the springs of 1993, 1994, and 1995, and several datasets of the complete BSF of sea ice were obtained. These experiments were conducted as part of the Office of Naval Research-sponsored program, Electromagnetic Properties of Sea Ice. The results of the 1995 experiment are used in the analysis presented here.

Instruments and methods

In collaboration with S. Pegau and R. Zaneveld of Oregon State University, instrumentation was developed for measuring beam attenuation in sea ice. The optical instrumentation was built by WET Labs, and a unique ice coring rig was built by the Polar Ice Coring Office (PICO), then at the University of Alaska, Fairbanks. After initial field trials, the optical instrumentation was modified for measuring the BSF in the manner illustrated in Fig. 1. The illustration shows how two holes are cored in the ice with a separation R, where R is defined as the horizontal distance through the ice separating the holes. A collimated light source, in this case a laser diode within a cylindrical housing, is lowered into one hole (left one in Fig. 1). An irradiance detector, also in a cylindrical housing, is lowered into the other hole and aligned with the axis of the source beam. As discussed above, the BSF is the irradiance distribution around a constant arc from a collimated source, as illustrated in the inset in Fig. 1. For an isotropic medium, it is entirely equivalent if the irradiance detector is kept fixed and the source is rotated. For example, in the inset of Fig. 1, if the beam is pointed at the position of $E(\theta)$, then the irradiance $E(0)$ will be identical to the irradiance at $E(\theta)$ when the source is pointing in its original direction. Therefore, as the source beam in the cylindrical housing on the left in Fig. 1 is rotated, the irradiance distribution recorded by the detector is BSF(θ).

The only assumption in this method is that the medium is isotropic, at least optically. It is well known that sea ice can be anisotropic due to the columnar alignment of the ice crystals during formation. Fractures in the ice, which can channel a light beam, also cause anisotropy. In general, however, the

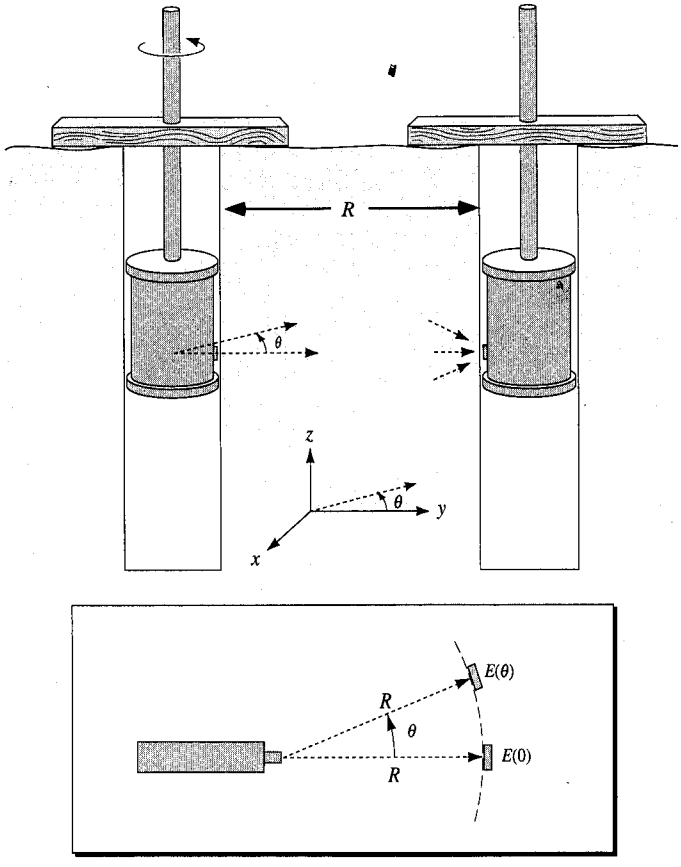

Fig. 1. Experimental setup for measuring the complete BSF of sea ice in situ.

anisotropic structures within sea ice should have a small effect on irradiance-level radiative transfer unless there is high spatial coherence in crystal alignment. The severity of anisotropic effects on the BSF measurements can be characterized in the following manner. By rotating the source beam counterclockwise (looking down), the BSF is measured from 0° to +180°, and by rotating it clockwise, the BSF is measured from 0° to −180°. If the medium is isotropic, a plot of the BSF from −180° to +180° should be a symmetric curve of ~0°. As shown below, anisotropic effects do show up in the data, but they are mainly local effects at discrete angles, probably due to light channeling from fractures. These discrete effects can easily be removed or smoothed out since the primary interest here is the overall shape of the BSF. In most cases, the overall shape of the BSF was found to be symmetric. Note that this test is a necessary, though not sufficient condition for proving isotropy.

The optical instrumentation consisted of separate source and detector units housed in water-tight canisters. The light source was a laser diode which emitted ~1 mW at a nominal wavelength of 670 nm. The beam had a nominal divergence of 3 mrad as specified by the manufacturer. The laser diode was electronically modulated for phase-synchronous detection with the photodetector. The signal from the photodetector was digitized within its housing and then recorded and displayed on a laptop computer. Both the source and detector housings were built out of a polycarbonate material and were designed to be water-tight since the ice holes sometimes fill with seawater. Unfortunately, this material did not hold up under the stress of the Arctic environment, and one of the canisters often leaked. The optical instrumentation did not incorporate an electronic means, such as an optical encoder, for recording the rotation angle. Thus, the BSF was measured at discrete angles, usually in 5° or 10° increments, and the angles were measured manually with a protractor and pointer. Approximately 25 to 50 digitized photodetector signals were recorded for each angle and averaged to produce a single value of the BSF at that angle.

The ice-coring rig, built by PICO, was specifically designed for the application of measuring in-ice optical properties. When set in place, the rig was able to core a series of holes over a total linear distance of ~1 m. The cores were ~15 cm in diameter. The purpose of drilling a series of holes was to make BSF measurements over several different pathlengths. This was accomplished by first drilling two holes with the largest desired separation, making the BSF measurement, and then drilling another hole between these two for a shorter pathlength BSF measurement. The process was repeated until the shortest desired pathlength was achieved, which was typically ~15 cm.

Results

The measurements presented here were made on shorefast first- and multiyear ice in the Chuckchi Sea near the coast of Barrow, Alaska, in April 1995. These data, although not extensive or comprehensive, have the greatest angular resolution and range (covering $-180° \leq \theta \leq +180°$) of the datasets obtained during the 1993, 1994, and 1995 Barrow experiments. Comparison of the 1995 data with the 1994 data over the limited angular range of −90° to +90° did not reveal any differences that affect the conclusions presented here. The 1993 experiment was preliminary for testing the experimental design and instrumentation. The coring rig, optical instruments, and associated equipment were towed to the sites with snowmobiles, where measurements were performed over the course of about a week. The most extensive measurements were made of first-year ice, although some measurements were obtained of a multiyear floe embedded in the first-year ice. BSF measurements were made both as a function of separation distance R and depth z within the ice. The angular range of the BSF measurements usually spanned from 0° to 180°, both clockwise and counterclockwise. Occasionally, time or equipment constraints restricted measurements to one direction, usually counterclockwise (looking down) from 0° to +180°, and in some instances measurements were made to only 90°. Unless stated otherwise, graphs are of data from the first-year ice site.

The BSF was usually measured in dry holes, although occasionally the holes flooded, either by seepage or because the holes were deliberately drilled down into the water. The inner walls of the holes were generally smooth, but certainly not to optical tolerances so that some effect was expected on the beam as it passed through the ice interface. But hole-surface roughness should generally cause only random effects that can be averaged out, and should not cause any

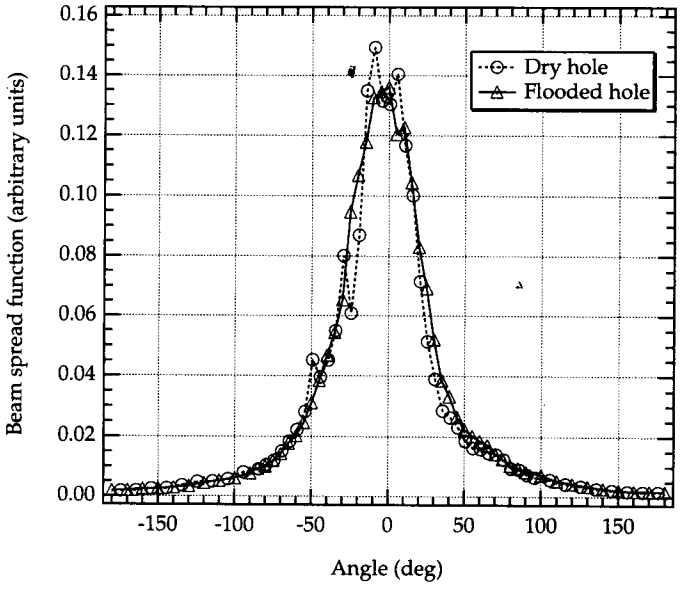

Fig. 2. Sea ice BSF with the holes dry and flooded with seawater. Pathlength through the ice was R = 30 cm.

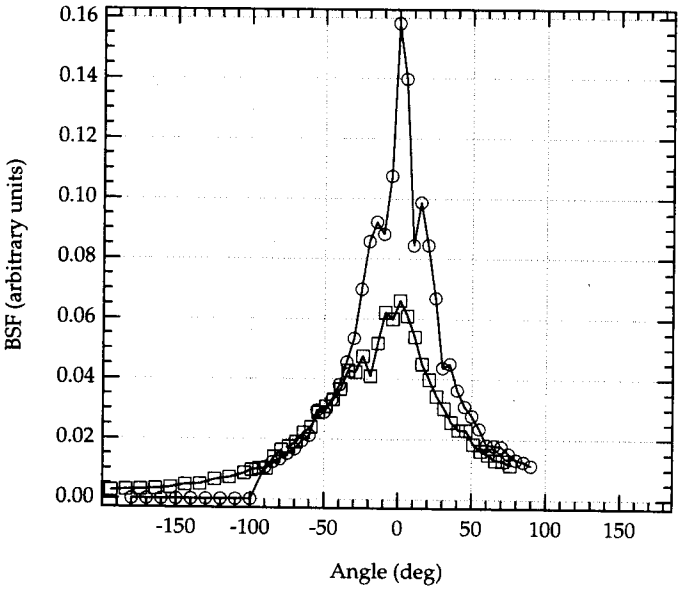

Fig. 3. Sea ice BSF of multiyear ice at two depths. Pathlength through the ice was R = 30 cm.

significant or systematic effect on the shape of the BSF. These effects should be greatest when the holes are dry due to the larger index of refraction change at the ice interface compared to when the holes are wet. Figure 2 shows two BSFs that were measured in the same hole at the same depth when the hole was dry and later flooded with seawater. The pathlength was R = 30 cm. Except for some random differences, the two curves are essentially identical. As expected, the curve with the most variability has the data from the dry hole. Some of the variability is also perhaps due to "light channeling" by fractures and brine pockets.

An important feature of all the sea ice BSFs that were measured is their broadness, or angular width, which indicates a high degree of scattering. Indeed, the irradiance of the scattered laser light could be measured when the detector was pointed at 180°. Figure 3 shows the BSF of a multiyear floe at two depths, with R = 30 cm. The broadness of these BSFs is again clearly evident and similar to the first-year ice BSFs. Compare this with the PSF, which is equivalent to the BSF, of ocean water (Fig. 4). The ocean water PSF was measured by one of the authors (R.A.M.) in Monterey Bay, California by using a method similar to that first described by Honey (1979) and later used by Voss and Chapin (1990) and Maffione et al. (1991). The ocean water PSF is so highly peaked that it must be graphed on a log plot. In the first 30° it decreases by four orders of magnitude, after which the dynamic range of the digital camera begins to be reached. In contrast, the sea ice BSF barely drops by one order of magnitude over 90°. Moreover, there is a large difference in pathlengths between the ocean water PSF and sea ice BSF. The pathlength of the ocean water PSF was 10 m, whereas the sea ice BSF pathlength was 0.30 m. Because multiple scattering increases with pathlength, the highly scattering nature of sea ice, when compared with ocean water at least, is quite dramatic.

Figure 5 shows a series of ice BSFs that were measured as a function of depth within the ice, with a pathlength between source and receiver of R = 30 cm. Again, the broad, bell-shaped–like curves are evident in all the BSFs. A visual examination of both the core and ice hole revealed layering of the ice sheet. Layers were identified by their slightly darker or more milky appearance compared with other regions of the ice sheet. There was some correlation between the BSF amplitudes and the ice layers, especially where the layer was very distinct, such as near the bottom of the ice sheet corresponding to the 106-cm BSF. The correlation of the BSF amplitudes with the other layers was not as pro-

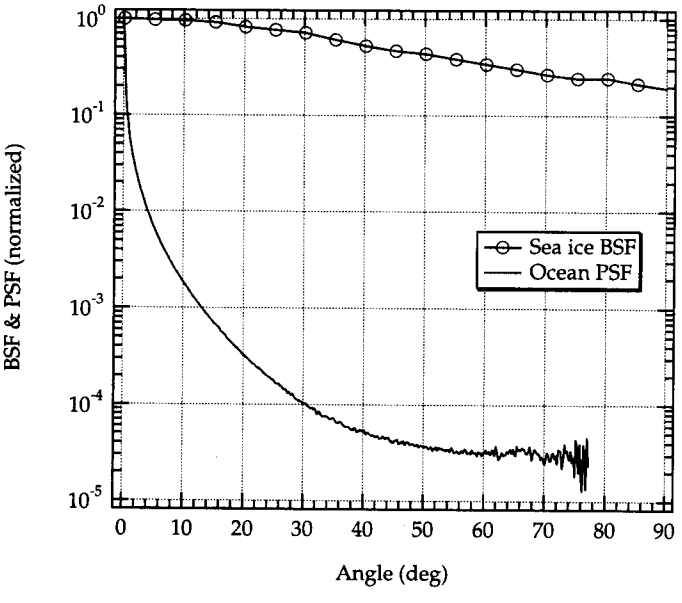

Fig. 4. Comparison of the BSF of sea ice and the equivalent PSF of ocean water. Sea ice pathlength was 30 cm; ocean water pathlength was 10 m.

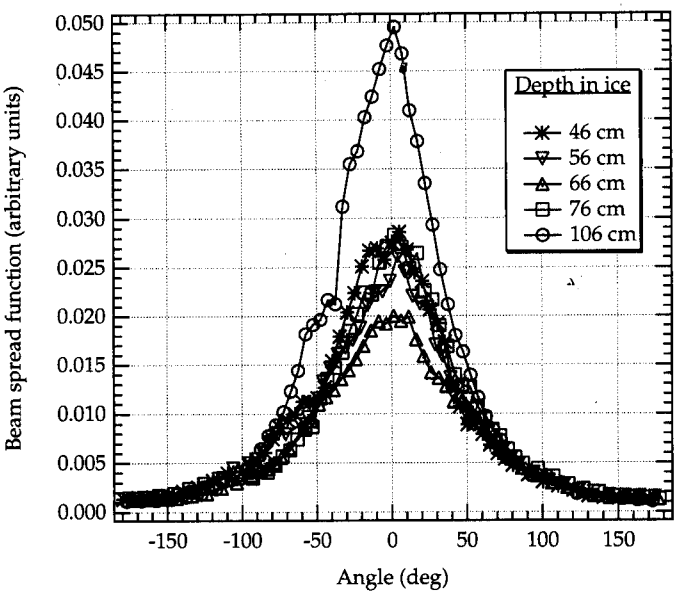

Fig. 5. The BSF as a function of depth in sea ice. Pathlength was $R = 30$ cm.

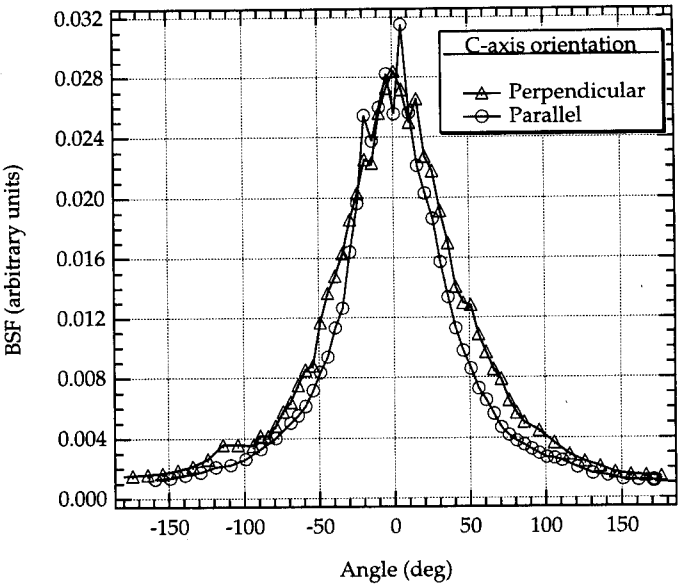

Fig. 6. The BSF for two different orientations of the 0°-beam axis with the C-axis of the ice crystals. Pathlength was $R = 30$ cm.

nounced, although this may have been due to the fact that the layers were not characterized in an independent, quantitative manner; layers were observed by visual inspection of the ice cores. No definitive correlation was found between the BSF shapes and the layers.

As already discussed, an important assumption in this technique for measuring the BSF is that the medium is isotropic, at least for light propagation at the irradiance level. Sea ice often forms anisotropic structures, most notably columnar crystals which may align in a predominant direction. Fractures, on certain spatial scales, are anisotropic structures as well. If the spatial coherence of these anisotropic structures is not highly pronounced, then anisotropic effects should average out at the irradiance level of light propagation. The data shown in Figs. 2, 3, and 5 are all relatively symmetric at ~0°, save for local variations at discrete angles. Indeed, an examination of all the measured BSFs revealed no systematic asymmetry.

Another dataset that supports the assumption of an isotropic medium for irradiance-level propagation is shown in Fig. 6. Here, one BSF was measured with the 0°-beam axis pointing in the direction of the ice C-axis, and the other BSF was measured with the 0°-beam axis perpendicular to the C-axis. The experimental arrangement consisted of three holes forming a right angle, with the laser in the vertex hole. Both measurements were made at the same depth (76 cm) and the same pathlength (30 cm). The two BSFs exhibit symmetry at ~0° and are similar both in shape and amplitude. It is difficult, however, to draw any definitive conclusions by comparing the parallel and perpendicular BSFs because differences may be due to local variability in the ice. Still, the consistent symmetry at $\sim\theta = 0°$ in all the BSFs, even when the 0°-beam axis was randomly oriented with respect to the ice C-axis, strongly supports the assumption that sea ice is an isotropic medium for irradiance-level propagation.

A potential source of experimental error is the finite size of the holes and instrumentation. In theory, the BSF is the irradiance distribution at a point in space generated by a point-collimated source. Although the source and detector apertures are small compared with other relevant dimensions, the rotation of the source about a total circumference of $2\pi \times 7.5$ cm $\cong 47$ cm introduces a potentially significant pathlength variation between source and detector. Ideally, one would like to measure the BSF using small-diameter holes whose size is insignificant compared with either a diffuse attenuation length, $1/K$, where K is the diffuse attenuation coefficient, or the distance R between the source and detector. Let the measured BSF be denoted BSF_m; then to first order, BSF_m can be corrected with the formula

$$\mathrm{BSF}(R, \theta) = \mathrm{BSF}_m(R, \theta)\exp(r - R)K, \quad (1)$$

where

$$r = \sqrt{d(d/2 + R)(1 - \cos\theta) + R^2}$$

is the linear distance between the source and detector and $d = 15$ cm is the diameter of the hole. Eq. 1 simply removes the irradiance attenuation due to the pathlength difference $r - R$.

To apply the BSF correction, the irradiance attenuation coefficient K needs to be known or estimated. It is defined by

$$K(r, \theta) \equiv \frac{-1}{\mathrm{BSF}(r, \theta)} \frac{\partial \mathrm{BSF}(r, \theta)}{\partial r},$$

so that

$$\mathrm{BSF}(r, \theta) = \mathrm{BSF}(r_0, \theta)\exp\left(-\int_{r_0}^{r} K(r', \theta)\, dr'\right). \quad (2)$$

In general, the irradiance attenuation of the direct beam will be larger than the irradiance attenuation of the multiply scattered light from the beam. In other words, $K(r, \theta)$ takes on

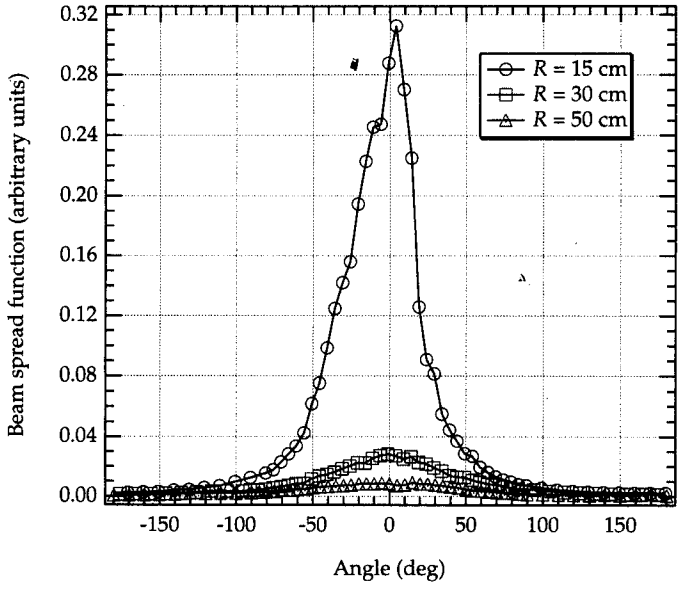

Fig. 7. BSF as a function of sea ice pathlength R.

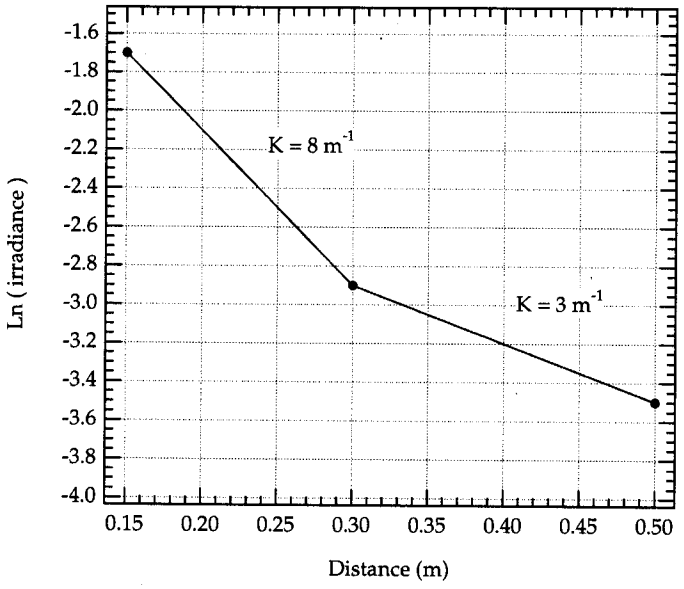

Fig. 8. Plot of ln[BSF(R, 0)] for the three BSFs in Fig. 7. K was computed with Eq. 3.

its maximum value at $\theta = 0°$. Moreover, as r increases, $K(r, \theta)$ will approach a constant for all θ, the asymptotic attenuation coefficient K_∞ (Preisendorfer 1959). $K(r, \theta)$ can be estimated from measurements of BSF(r, θ) at two discrete pathlengths r_1 and r_2 by

$$K(r, \theta) \cong \frac{\ln[\mathrm{BSF}(r_1, \theta)] - \ln[\mathrm{BSF}(r_2, \theta)]}{r_2 - r_1}. \quad (3)$$

At $\theta = 0°$, no BSF correction is required since $r = R$. The most accurate estimate of $K(r, \theta)$ is thus expected to be when $\theta = 0°$. A series of BSF measurements (Fig. 7) were made at three pathlengths, R = 15, 30, and 50 cm. Figure 8 shows a plot of ln[BSF(R, 0)] vs. R, from which K was estimated for the two regions, 15–30 and 30–50 cm. As expected, K decreases as R increases. Indeed, this rather dramatic decrease, from $K = 8$ m^{-1} to 3 m^{-1} over a change in R of only 35 cm again illustrates the highly scattering nature of sea ice.

The BSF correction (Eq. 1) becomes more significant as K increases and R decreases. Thus, for the present data, the largest correction is for $R = 15$ cm and $K = 8$ m^{-1}. Figure 9 shows the corrected and uncorrected BSF for $R = 15$ cm, using a constant value of $K = 8$ m^{-1}. The correction at small angles is insignificant, since $r \cong R$, and becomes noticeable only at large angles. Nonetheless, the overall shape of the BSF is still not significantly altered. Also, the correction at larger angles is certainly overestimated because, as already noted, $K(r, \theta) < K(R, 0)$. Indeed, it is likely that $K(r, \theta) \cong K_\infty$ since the BSF at angles other than 0° is diffuse irradiance due to multiply scattered photons. When $K = 3$ m^{-1} was used for $\theta > 30°$, the BSF correction was insignificant. For $R \geq 30$ cm, the BSF correction was negligible even when values of $K > 3$ m^{-1} were used. The conclusion is that the finite size of the instrumentation does not cause any significant change in the measured BSFs, and the correction can be ignored, at least for the present data.

The apparent bell-shaped curve of the BSFs shown in the previous figures suggests a Gaussian function for fitting the data. Schoonmaker et al. (1989) used a Gaussian function to fit their laboratory BSF data, which, as described earlier, was actually a paraxial approximation to the BSF as defined by Mertens and Replogle (1977). A least-squares regression of the BSF data in Fig. 6 to the Gaussian function

$$\mathrm{Gauss}(\theta) = A \exp\left(-\frac{\theta^2}{2\sigma^2}\right) \quad (4)$$

is shown in Fig. 10. For clarity, only one BSF (perpendic-

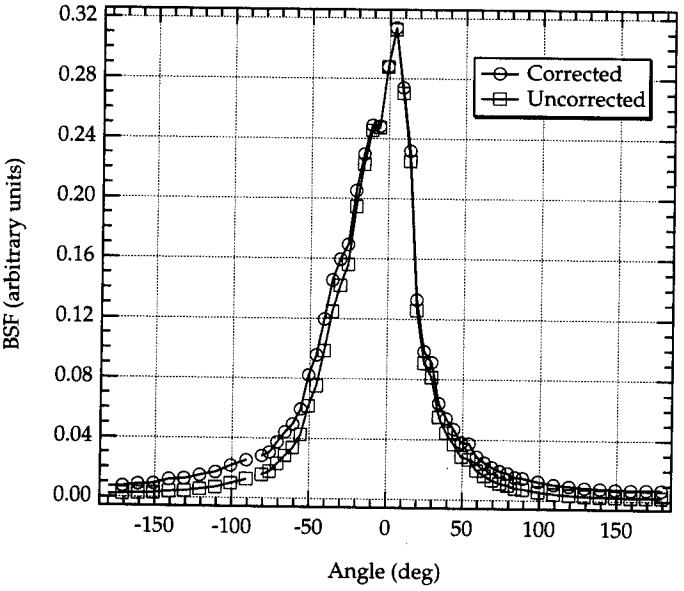

Fig. 9. Result of applying the correction (Eq. 1) to the 15-cm pathlength BSF data in Fig. 7. This is the most extreme correction and is likely overestimated. For BSF data where $R > 15$ cm, the correction was negligible.

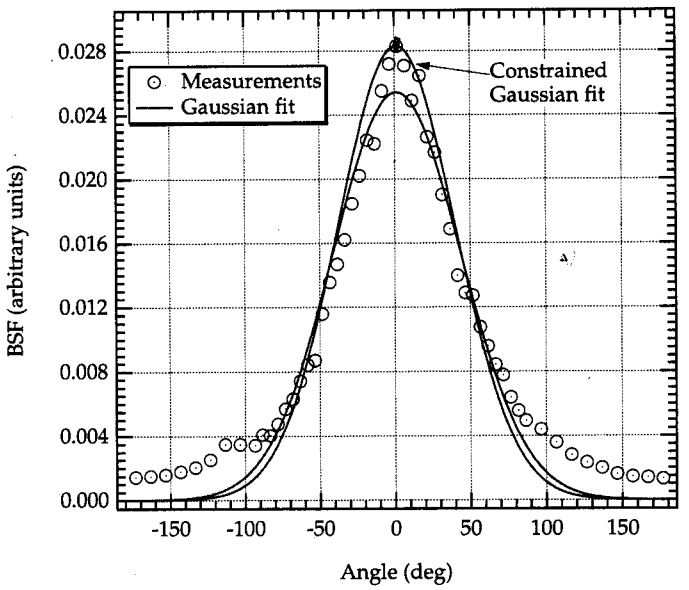

Fig. 10. Constrained and unconstrained regressions to the BSF in Fig. 6 (perpendicular) using the Gaussian function (Eq. 6).

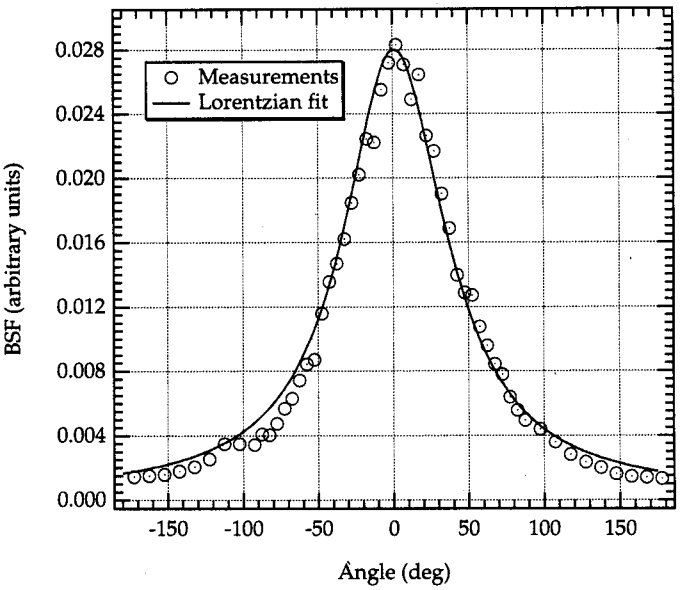

Fig. 11. Result of regressing the BSF data in Fig. 10 to a Lorentzian function (Eq. 5).

ular) is shown, but the results were similar for the other BSF (parallel) as well. Two regressions were performed and shown as the solid curves in Fig. 10. In one of the regressions, A and σ were both free parameters, and in the other regression A was constrained to the peak value of the BSF data. The best fit occurred when the Gaussian function was constrained to one free parameter, the standard deviation σ. Nonetheless, even a constrained Gaussian function did not seem to adequately describe any of the BSF data, especially at angles greater than ~80°, which is clearly evident in Fig. 10.

It was found that all of the BSF data regressed extremely well, over the full angular range, to a Lorentzian function, which can be expressed in the form

$$\mathrm{Lor}(\theta) = \frac{A}{[(\theta/\sigma)^2 + 1]'} \tag{5}$$

where A is the maximum value at $\theta = 0°$ and σ is the half-maximum angle. Figure 11 shows the results of fitting a Lorentzian function to the same data used in the Gaussian fit shown in Fig. 10. In the Lorentzian fit, both A and σ were free parameters and the regression gave the values $A = 0.028$ and $\sigma = 41°$. For the other BSF, where the 0°-beam axis was oriented parallel to the ice C-axis, the regression gave the values $A = 0.029$ and $\sigma = 32°$. The difference in the widths, σ, is most likely due to a difference in the two volumes of ice rather than a C-axis orientation effect, although this possibility can not be entirely discounted.

The Lorentzian function is useful for fitting the BSF data to compare their half-maximum angles σ. For example, a regression to the Lorentzian function (Eq. 5) with the three BSFs in Fig. 7 yielded the σ values 22°, 42°, and 47°, corresponding to the pathlengths 15, 30, and 50 cm, respectively. The increasing width of the BSF with increasing pathlength is due to multiple scattering, but it is again the highly scattering nature of sea ice that rapidly increases the BSF width over such relatively short pathlengths. A 200% change in σ occurred over a 15-cm change in R, from 15 to 30 cm. Note, however, that the next 20-cm change in R, from 30 to 50 cm, yielded a 12% change in σ. This sharply decreasing change in σ indicates the rapid approach, over relatively short geometrical distances, of the BSF toward its asymptotic, constant shape.

Discussion

The ultimate objective of the present work is to better understand the optical nature of sea ice and to develop practical models for describing and predicting radiative transfer in sea ice. The physically complex nature of sea ice makes modeling it from first principles nearly impossible. Moreover, single scattering approximations cannot be used because, as shown above and by the work of others, sea ice is a highly scattering medium. This also complicates the direct measurement of IOPs. The highly scattering nature of sea ice may, however, allow for the application of some useful simplifications in the theory of radiative transfer.

Asymptotic radiative transfer theory predicts that the radiance distribution, once asymptotic, does not change its shape and decays in amplitude as $\exp(-K_\infty R)$, where K_∞ is the asymptotic attenuation coefficient. The theory also predicts that both the shape of the radiance distribution and K_∞ are functions of only the IOPs of the medium and are independent of the boundary conditions (Priesendorfer 1959). Thus, for a given set of IOPs, the asymptotic radiance distribution and K_∞ are uniquely given regardless if the light field is generated by solar illumination or a submerged source. Therefore, the asymptotic radiance distribution due to a submerged source is identical to the asymptotic radiance distribution for plane wave illumination at the boundary of

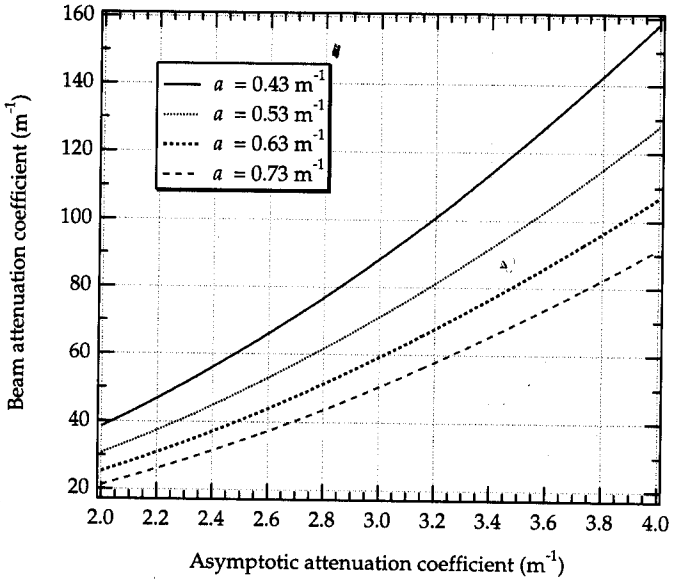

Fig. 12. Computation of $c = a + b$ as a function of K_∞, for four values of a, using Eq. 7 to calculate b.

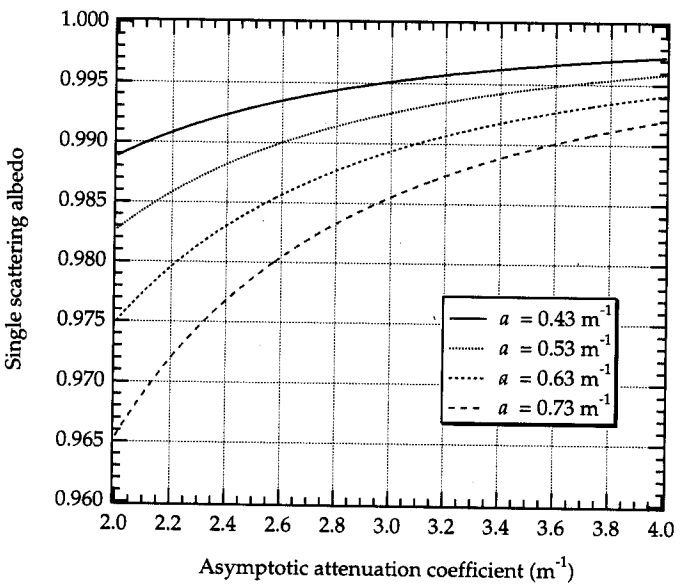

Fig. 13. Computation of $\varpi_0 = b/c$ as a function of K_∞ using Eq. 7 to calculate b. The same four values of a are used as in Fig. 12.

the medium, such as solar illumination on the surface of the ocean, or in this case sea ice.

As explained earlier, the PSF is the radiance distribution due to a Lambertian source and, by reciprocity, so is the BSF. The sea ice BSF measurements are thus equivalent to the in-ice radiance distribution due to a submerged Lambertian source. In general, sea ice is a far more highly scattering medium than ocean water, so that the asymptotic state is approached much more rapidly in sea ice. This is true not only in terms of geometrical distance, but also in terms of optical pathlength $\tau \equiv R/c$, where c is the beam-attenuation coefficient. Over a given optical pathlength, more scattering events occur in a medium with a high single-scattering albedo $\omega_0 = b/c$, where b is the total scattering coefficient, than in a medium with a lower ω_0. How far from the source the light field becomes asymptotic, in terms of τ, depends mainly on ω_0, and to a lesser extent on the scattering phase function (Gordon et al. 1993). But in terms of geometrical distance R, the dependence is mainly on the absolute value of b.

The BSF measurements as a function of pathlength (Fig. 7) strongly suggest that the BSF is closely approaching the asymptotic radiance distribution for $R > 30$ cm. As shown in Fig. 8, the irradiance attenuation appears to be approaching an asymptotic limit that is probably close to $K = K_\infty \cong 2$ m^{-1}. The change in the shape of the BSF, as measured by σ, is also rapidly approaching an asymptote. As noted earlier, σ changed by 200% from 15 to 30 cm, but then changed by only 12% from 30 to 50 cm. The definitive test is to compare the BSF to the asymptotic radiance distribution, $L_\infty(\theta)$, for the appropriate choice of IOPs. $L_\infty(\theta)$ is uniquely determined by ω_0 and the scattering phase function, $\tilde{\beta}(\psi)$, where ψ is the scattering angle.

The asymptotic radiance distribution, $L_\infty(\theta)$, can be computed accurately using an eigenmatrix method that is incorporated into a numerical radiative transfer model called Hydrolight (Mobley 1994). To properly compare $L_\infty(\theta)$ with the BSF, ω_0 and $\tilde{\beta}(\psi)$ of the sea ice needs to be known or estimated. From Monte Carlo radiative transfer calculations of highly turbid water, Kirk (1994) found that K_∞ can be accurately related to a, the absorption coefficient, and b by

$$K_\infty = \sqrt{a^2 + Gab}, \tag{6}$$

where G is a regression parameter. Kirk reported the value of $G = 0.233$ for the highly scattering cases, and for all cases that covered the range $0.5 \leq \omega_0 \leq 0.995$, he reported an average value of $\bar{G} = 0.245$. Based on the results shown in Fig. 7, K likely falls within the range 8 m$^{-1} \leq K \leq 2$ m$^{-1} \cong K_\infty$, with the lower value applying to $R > 50$ cm.

At 670 nm, a for ocean water is predominantly determined by pure-water absorption and, to a lesser degree, by chlorophyll, except when concentrations are extremely high. For pure water, $a(670) \cong 0.43$ m^{-1} (Smith and Baker 1981). Although phytoplankton were embedded in the ice, their concentrations were not high and probably contributed no more than 0.2 m^{-1}, and at most 0.3 m^{-1}, to $a(670)$. Thus, for sea ice, a reasonable range for $a(670)$ is 0.43 m$^{-1} \leq a \leq 0.73$ m^{-1}. The temperature dependence of $a(670)$ is negligible (Trabjert and Højerslev 1996), especially compared with the variability in phytoplankton absorption.

Solving Eq. 6 for b gives

$$b = \frac{K_\infty^2 - a^2}{Ga}, \tag{7}$$

which is used to compute $c = a + b$ and $\omega_0 = b/c$. The beam-attenuation coefficient c is plotted in Fig. 12 for different values of a spanning the range 0.43 m$^{-1} \leq a \leq 0.73$ m^{-1}, with $G = 0.233$. For K_∞ between 2 and 3 m^{-1}, c ranges from 20 to 90 m^{-1}. Assuming a likely value of $a(670) \cong 0.53$ m^{-1} gives $c \cong 50$ m^{-1} for $K_\infty = 2.5$ m^{-1}. Plots of ω_0

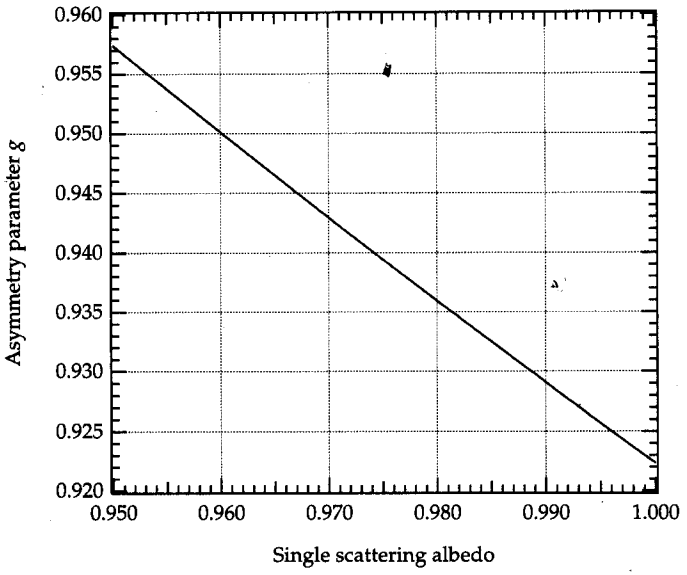

Fig. 14. Asymmetry parameter g computed with Eq. 10 using $G = 0.233$.

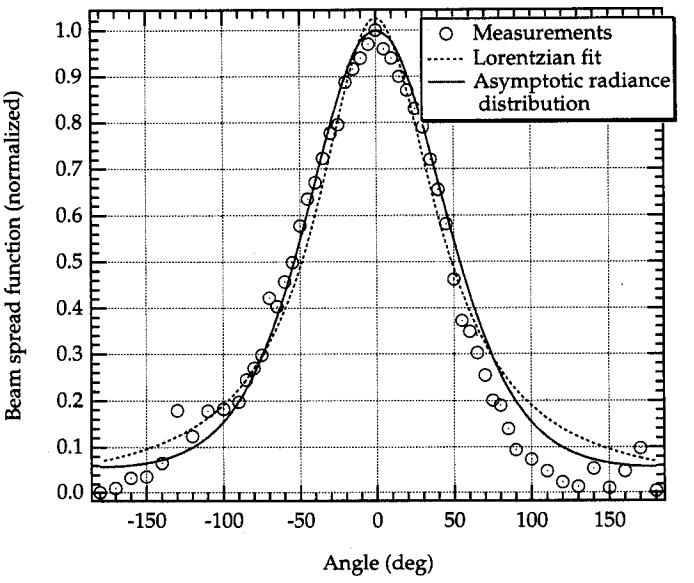

Fig. 15. Comparison of computed asymptotic radiance distribution with the measured BSF for the pathlength $R = 50$ cm.

are shown in Fig. 13 for the same four values of a used for Fig. 12. The results confirm that $\omega_0 > 0.95$, and is probably >0.98 for the likely values of a and K_∞.

The remaining IOP to be estimated is the scattering phase function $\tilde{\beta}(\psi)$. Because the inhomogeneities in sea ice that cause scattering are predominantly large compared to visible wavelengths, $\tilde{\beta}(\psi)$ is expected to be a highly forward-peaked scattering-phase function. Measurements of scattering by ice confirm this (Grenfell and Hedrick 1983; Miller et al. 1994). A useful form for $\tilde{\beta}(\psi)$ is the Henyey-Greenstein (1941) phase function, namely

$$\tilde{\beta}(\psi) = \frac{1}{4\pi} \frac{1 - g^2}{(1 + g^2 - 2g \cos \psi)^{3/2}}, \tag{8}$$

where g is the average cosine of the scattering angle for $\tilde{\beta}(\psi)$, otherwise known as the asymmetry parameter, defined by

$$g \equiv 2\pi \int_{-1}^{1} \tilde{\beta}(\psi) \cos \psi \, \mathrm{d}(\cos \psi).$$

Monte Carlo calculations of radiative transfer in the ocean show that irradiance propagation is only weakly dependent on the shape of $\tilde{\beta}(\psi)$ in the near-forward direction ($<30°$) (Gordon 1993). Therefore, K_∞ should not be a strong function of $\tilde{\beta}(\psi)$, nor should the shape of the asymptotic radiance distribution $L_\infty(\theta)$, since it consists only of photons that have scattered at least once, and more likely have undergone many scattering events. Regardless of the fine details of $\tilde{\beta}(\psi)$, the Henyey-Greenstein phase function (Eq. 8) should be adequate for irradiance-level and asymptotic computations of the light field in sea ice.

It remains then to estimate g, the asymmetry parameter of the phase function. As previously shown, ω_0 of sea ice is generally >0.95, and is likely ≥ 0.98 for the sea ice of which the BSF measurements were made. The high ω_0 of sea ice suggests that photon diffusion theory may adequately describe radiative transfer in sea ice at a sufficient distance from boundaries, where "sufficient" means close to the asymptotic state. In the asymptotic limit, photon diffusion theory predicts that

$$K_\infty = \sqrt{3a(c - gb)}. \tag{9}$$

(*See* Maffione [1998] for a complete derivation and discussion of this equation.) Equating Eq. 9 to Kirk's result (Eq. 6) and solving for g gives

$$g = \frac{2/\omega_0 - G + 1}{3}, \tag{10}$$

which is plotted in Fig. 14 over the range $0.95 \leq \omega_0 \leq 1$. For $\omega_0 \cong 0.98$, Eq. 10 predicts $g \cong 0.935$.

The asymptotic radiance distribution was computed with Hydrolight using an Henyey-Greenstein phase function with $g = 0.935$, $\omega_0 = 0.98$, and $a = 0.58$ m^{-1}. Figure 15 shows the results, with $L_\infty(\theta)$ plotted over the BSF measured at $R = 50$ cm. The dotted line is the regression of the data to a Lorentzian function (Eq. 5). Clearly, $L_\infty(\theta)$ matches the BSF quite well and confirms that the BSF is indeed closely approaching the asymptotic radiance distribution.

Conclusions

A new method for measuring profiles of the BSF of sea ice also yields the complete (axially symmetric) radiance distribution due to a submerged Lambertian source. The BSF of sea ice is significantly different than the BSF of ocean water owing to the highly scattering nature of sea ice. Based on an equation developed by Kirk for highly turbid water, and estimates of K_∞ and a for sea ice in the visible spectrum, sea ice can generally be expected to have a single scattering albedo $\omega_0 > 0.97$. The high ω_0 of sea ice suggests that photon diffusion theory can adequately describe radiative trans-

fer in sea ice, at least at the irradiance level. Combining a result of this theory with Kirk's equation predicts that the asymmetry parameter g of the scattering-phase function is approximately in the range $0.9 \leq g \leq 0.95$. An exact computation of the asymptotic radiance distribution matched quite well the measured BSF at a pathlength of 50 cm, strongly suggesting that the BSF rapidly approaches, over geometrical distances, the asymptotic radiance distribution. Thus, for sufficient pathlengths, both asymptotic radiative transfer theory and photon diffusion theory can be used to interpret BSF measurements of sea ice. Application of these theories provide useful relationships for estimating sea ice IOPs, such as K_∞, ω_0, and g.

References

GILBERT, G. D., AND R. R. BUNTZEN. 1986. In-situ measurements of the optical properties of Arctic sea ice, p. 252–263. *In* M. A. Blizard [ed.], Ocean optics VIII. Proc. SPIE **637**.

GORDON, H. R. 1993. Sensitivity of radiative transfer to small-angle scattering in the ocean: Quantitative assessment. Appl. Opt. **32:** 7505–7511.

———. 1994. Equivalence of the point and beam spread function of scattering media: A formal demonstration. Appl. Opt. **33:** 1120–1122.

———, K. DING, AND W. GONG. 1993. Radiative transfer in the ocean: Computations relating to the asymptotic and near-asymptotic daylight field. Appl. Opt. **32:** 1606–1619.

GRENFELL, T. C. 1991. Radiative transfer model for sea ice with vertical structure variations. J. Geophys. Res. **96:** 16,991–17,001.

———, AND D. HEDRICK. 1983. Scattering of visible and near infrared radiation by NaCl ice and glacier ice. Cold Reg. Sci. Technol. **8:** 119–127.

———, AND G. A. MAYKUT. 1977. The optical properties of ice and snow in the Arctic Basin. J. Glaciol. **18:** 445–463.

———, AND D. K. PEROVICH. 1981. Radiation absorption coefficients of polycrystalline ice from 400–1400 nm. J. Geophys. Res. **86:** 7447–7450.

HENYEY, L. C., AND J. L. GREENSTEIN. 1941. Diffuse radiation in the galaxy. Astrophys. J. **93:** 70–83.

HONEY, R. C. 1979. Beam spread and point spread function and their measurement in the ocean, p. 242–248. *In* S. Q. Duntley [ed.], Ocean optics VI. Proc. SPIE **208**.

JOELSON, B. D. 1996. Multiple scattering effects on pulse propagation in optically turbid media. Ph.D. thesis, Texas A&M Univ.

KIRK, J. T. O. 1994. Estimation of the absorption and the scattering coefficients of natural waters by use of underwater irradiance measurements. Appl. Opt. **33:** 3276–3278.

LIGHT, B. 1995. A structural-optical model of cold sea ice. M.S. thesis, Univ. Wash. 146 p.

LONGACRE, J. R., AND M. A. LANDRY. 1994. In-situ measurements of optical scattering from the water–ice interface of sea ice, p. 944–953. *In* J. S. Jaffe [ed.], Ocean optics XII. Proc. SPIE **2258.**

MAFFIONE, R. A. 1998. Theoretical developments on the optical properties of highly turbid waters and sea ice. Limnol. Oceanogr. **43:** 29–33.

———, D. R. DANA, AND R. C. HONEY. 1991. Instrument for underwater measurement of optical backscatter, p. 173–184. *In* R. W. Spinrad [ed.], Underwater imaging, photography, and visibility. Proc. SPIE **1537.**

———, K. J. VOSS, AND R. C. HONEY. 1993. Measurement of the spectral absorption coefficient in the ocean with an isotropic source. Appl. Opt. **32:** 3273–3279.

MAYKUT, G. A., AND T. C. GRENFELL. 1975. The spectral distribution of light beneath first-year sea ice in the Arctic Ocean. Limnol. Oceanogr. **20:** 554–562.

MERTENS, L. E., AND F. S. REPLOGLE, JR. 1977. Use of the point spread function for analysis of imaging systems in water. J. Opt. Soc. Am. **67:** 1105–1117.

MILLER, D., M. S. QUINBY-HUNT, AND A. J. HUNT. 1994. Polarization-dependent measurement of light scattering in sea ice, p. 908–919. *In* J. S. Jaffe [ed.], Ocean optics XII. Proc. SPIE **2258.**

MOBLEY, C. D. 1994. Light and water: Radiative transfer in natural waters. Academic.

MOORE, C. A. 1985. Development and testing of specialized instrumentation for the measurement of beam-spread function. SRI project 8266, final report.

PEROVICH, D. K., AND J. W. GOVONI. 1991. Absorption coefficients of ice from 250 to 400 nm. Geophys. Res. Lett. **18:** 1233–1235.

———, AND A. J. GOW. 1991. A statistical description of the microstructure of young sea ice. J. Geophys. Res. **96:** 16,943–16,953.

———, AND T. C. GRENFELL. 1981. Laboratory studies of the optical properties of young sea ice. J. Glaciol. **27:** 331–346.

———, AND ———. 1982. A theoretical model of radiative transfer in young sea ice. J. Glaciol. **28:** 341–357.

———, G. A. MAYKUT, AND T. C. GRENFELL. 1986. Optical properties of ice and snow in the polar oceans: I. Observations, p. 232–241. *In* M. Blizard [ed.], Ocean optics VIII. Proc. SPIE **637**.

PREISENDORFER, R. W. 1959. Theoretical proof of the existence of characteristic diffuse light in natural waters. J. Mar. Res. **18:** 1–9.

ROESLER, C. S., AND R. ITURRIAGA. 1994. Absorption properties of marine-derived material in Arctic sea ice, p. 933–943. *In* J. S. Jaffe [ed.], Ocean optics XII. Proc. SPIE **2258**.

SCHOONMAKER, J. S., K. J. VOSS, AND G. D. GILBERT. 1989. Laboratory measurements of optical beams in young sea ice. Limnol. Oceanogr. **34:** 1606–1613.

SMITH, R. C., AND K. S. BAKER. 1981. Optical properties of the clearest natural waters (200–800 nm). Appl. Opt. **20:** 177–184.

TANIS, F. J. 1994. Use of beam spreading measurements to estimate volume scattering properties in sea ice, p. 965–973. *In* J. S. Jaffe [ed.], Ocean optics XII. Proc. SPIE **2258**.

TRABJERT, I., AND N. K. HØJERSLEV. 1996. Temperature influence on light absorption by fresh water and seawater in the visible and the near-infrared spectrum. Appl. Opt. **35:** 2653–2658.

VOSS, K. J. 1991. Variation of the point spread function in the Sargasso Sea, p. 97–103. *In* R. W. Spinrad [ed.], Underwater imaging, photography, and visibility. Proc. SPIE **1537**.

———, AND A. L. CHAPIN. 1990. Measurement of the point spread function in the ocean. Appl. Opt. **29:** 3638–3642.

———, R. C. HONEY, G. D. GILBERT, AND R. R. BUNTZEN. 1992. Measuring the point spread function of sea ice in-situ, p. 517–526. *In* G. D. Gilbert [ed.], Ocean optics XI. Proc. SPIE **1750**.

WELLS, W. H. 1969. Loss of resolution in water as a result of multiple small-angle scattering. J. Opt. Soc. Am. **59:** 686–691.

Received: 25 October 1996
Accepted: 16 June 1997
Amended: 2 August 1997